

Simulation and detection of Dirac fermions with cold atoms in an optical lattice

Shi-Liang Zhu^{1,3}, Baigeng Wang², and L.-M. Duan³

¹*ICMP and LPIT, Department of Physics, South China Normal University, Guangzhou, China*

²*National Laboratory of Solid State Microstructures and Department of Physics, Nanjing University, Nanjing, China*

³*FOCUS Center and MCTP, Department of Physics, University of Michigan, Ann Arbor, MI 48109*

We propose an experimental scheme to simulate and observe relativistic Dirac fermions with cold atoms in a hexagonal optical lattice. By controlling the lattice anisotropy, one can realize both massive and massless Dirac fermions and observe the phase transition between them. Through explicit calculations, we show that both the Bragg spectroscopy and the atomic density profile in a trap can be used to demonstrate the Dirac fermions and the associated phase transition.

PACS numbers: 05.30.Fk, 03.65.Pm, 31.30.Jv, 73.43.Nq

Control of ultracold atoms in an optical lattice opens up many avenues to explore some fundamental phenomena at the forefront of condensed matter physics [1, 2, 3, 4, 5]. By designing configurations of this atomic system, one can simulate effective theories that are very different from the microscopic atomic physics. In this paper, we add an unusual example to the avenues of quantum simulation by showing that ultracold atoms in an optical lattice can be used to investigate physics associated with relativistic Dirac fermions. The ultracold atomic gas, as the coldest setup in the universe, is one of the most non-relativistic systems. Nevertheless, we will see that effective theories for the quasiparticles in this system can become relativistic under certain conditions.

We simulate Dirac fermions with single-component cold atoms in a two-dimensional hexagonal lattice. This lattice can be formed through interference of three laser beams, as we show below. The physics here is closely related to the properties of electrons in the graphene material formed with a single layer of carbon atoms [6, 7, 8, 9, 10, 11, 12]. The graphene, with its emergent relativistic massless quasiparticles, has recently raised strong interest in condensed-matter physics [6, 7, 9, 10, 11, 12]. Compared with the graphene, the system with cold atoms in an optical lattice may offer more controllability. For instance, we show that one can realize both massive and massless Dirac fermions by controlling anisotropy of the optical lattice. This anisotropy can be conveniently tuned through variation of the trapping laser intensity. Under such a tuning, one can also observe a quantum phase transition in this system. This phase transition is not associated with any usual symmetry breaking, but instead it is characterized by a topological change of the fermi surfaces [13, 14]. To detect the massive and the massless Dirac fermions and the phase transition between them, we calculate the Bragg spectrum for this system as well as its atomic density profile in a trap. From this calculation, we show that the conventional atomic detection techniques based on the Bragg spectroscopy [15] or the density profile measurement [1, 16, 17] can be used to demonstrate the Dirac fermions and the phase transition.

For cold atoms, one realizes an effectively two-

dimensional system by raising the potential barrier of the optical lattice along the z direction to suppress the vertical tunneling between different planes. Then, in the x-y plane, one can form a hexagonal optical lattice with three laser beams. For instance, as shown in Ref. [4], with three detuned standing-wave laser, the optical potential is given by

$$V(x, y) = \sum_{j=1,2,3} V_j \sin^2[k_L(x \cos \theta_j + y \sin \theta_j) + \pi/2] \quad (1)$$

where $\theta_1 = \pi/3$, $\theta_2 = 2\pi/3$, $\theta_3 = 0$, and k_L is the optical wave vector. If $V_1 = V_2 = V_3$, the energy contour of the potential $V(x, y)$ is shown in Fig. 1(a), where its minima (marked with the solid dots) form a standard hexagonal lattice. It is easy to tune the potential barriers V_j by variation of the laser intensities along different directions. With different V_j , one can still get a hexagonal lattice but with a finite anisotropy. For instance, Figure 1(b) shows the potential contour with $V_1 = V_2 = 0.91V_3$, where the neighboring sites along the horizontal direction have a larger distance and a higher barrier. As the atomic tunneling rate in an optical lattice is exponentially sensitive to the potential barrier, this control provides an effective method to tune the anisotropy of the atomic tunneling rate in this lattice.

A hexagonal lattice consists of two sub-lattices denoted by A and B as shown in Fig. 1(c). We consider single-component fermionic atoms (e.g., ^{40}K , ^6Li etc.) in this hexagonal lattice. For single-component fermions, the atomic collisions are negligible at low temperature. The Hamiltonian is given by the simple form

$$H = - \sum_{\langle i, j \rangle} t_{ij} (a_i^\dagger b_j + h.c.), \quad (2)$$

where $\langle i, j \rangle$ represents the neighboring sites, and a_i and b_j denote the fermionic mode operators for the sub-lattices A and B, respectively. The tunneling rates t_{ij} in general depend on the tunneling directions in an anisotropic hexagonal lattice, and we denote them as t_1, t_2, t_3 corresponding to the three different directions (see Fig. 1(c)). In this work, for simplicity, we assume

$t_1 = t_2 = t$ and $t_3 = \beta t$, where $\beta > 0$ is the anisotropy parameter. In the following, we show that by tuning the anisotropy β , the quasiparticles in this system change their behaviors from massless to massive Dirac fermions, with a quantum phase transition between the two cases.

The Hamiltonian (2) can be diagonalized with a simple extension of the method for the graphene material [12]. For the sub-lattice A , the positions of the sites can be expressed as $\mathbf{A} = m_1 \mathbf{a}_1 + m_2 \mathbf{a}_2$, where m_1 and m_2 are integers, and the basis vectors $\mathbf{a}_1 = (\sqrt{3}, -1)(a/2)$, $\mathbf{a}_2 = (0, a)$ ($a = 2\pi/(\sqrt{3}k_L)$ is the lattice spacing). The sites in the sub-lattice B are generated by a shift $\mathbf{B} = \mathbf{A} + \mathbf{b}$ with three possible shift vectors $\mathbf{b}_1 = (1/\sqrt{3}, 1)(a/2)$, $\mathbf{b}_2 = (1/\sqrt{3}, -1)(a/2)$, and $\mathbf{b}_3 = (-a/\sqrt{3}, 0)$ (see Fig. 1(c)). The first Brillouin zone of this system also has a hexagonal shape in the momentum space with opposite sides identified but rotated an angle of $\pi/6$ relative to the hexagon of the real-space lattice (see Fig. 1(d)). Corresponding to two different sites A and B in each cell in real hexagonal lattice, only two of the six corners in Fig. 1(d) are inequivalent, usually denoted as K and K' . One can choose $\mathbf{K} = (2\pi/a)(1/\sqrt{3}, 1)$ and $\mathbf{K}' = -\mathbf{K}$. With a Fourier transform $a_i^\dagger = \frac{1}{\sqrt{N}} \sum_{\mathbf{k}} \exp(i\mathbf{k} \cdot \mathbf{A}_i) a_{\mathbf{k}}^\dagger$ and $b_j^\dagger = \frac{1}{\sqrt{N}} \sum_{\mathbf{k}} \exp(i\mathbf{k} \cdot \mathbf{B}_j) b_{\mathbf{k}}^\dagger$, where N is the number of sites of the sub-lattice A (or B), the Hamiltonian (2) simplifies to $H = \sum_{\mathbf{k}} [\phi(\mathbf{k}) a_{\mathbf{k}}^\dagger b_{\mathbf{k}} + h.c.]$, where $\phi(\mathbf{k}) = -\sum_{s=1}^3 t_s \exp(i\mathbf{k} \cdot \mathbf{b}_s)$. The energy eigenvalues of H are given by $E_{\mathbf{k}} = \pm |\phi(\mathbf{k})|$, which has the expression

$$E_{\mathbf{k}} = \pm t \sqrt{2 + \beta^2 + 2 \cos(k_y a) + 4\beta \cos(\sqrt{3} k_x a/2) \cos(k_y a/2)}. \quad (3)$$

The energy versus the momentum from Eq.(3) is plotted in Fig. 1(e) and 1(f) for different values of the anisotropy β . There are two branches of curves corresponding to the \pm sign in Eq. (3). When $0 < \beta < 2$, the two branches touch each other, and around the touching points there appears a Dirac cone structure. One has the standard cone same as the graphene material with $\beta = 1$ [6, 7, 12], and as β deviates from 1, the cones squeeze in x or y direction, but they still touch each other. When $\beta > 2$, the two branches separate with a finite energy gap $\Delta = |t|(\beta - 2)$ between them. So, across the point $\beta = 2$, the topology of the fermi surface changes and there is a corresponding quantum phase transition, albeit no symmetry breaks at this point. With this phase transition, the system changes its behavior from a semi-metal to an insulator at the half filling case (half filling means one atom per cell; note that each cell has two sites). Around the half filling, the fermi surface is close to the touching points and one can expand the momentum \mathbf{k} around one of the touching points (k_x^0, k_y^0) as $(k_x, k_y) = (k_x^0 + q_x, k_y^0 + q_y)$. Up to the second order of

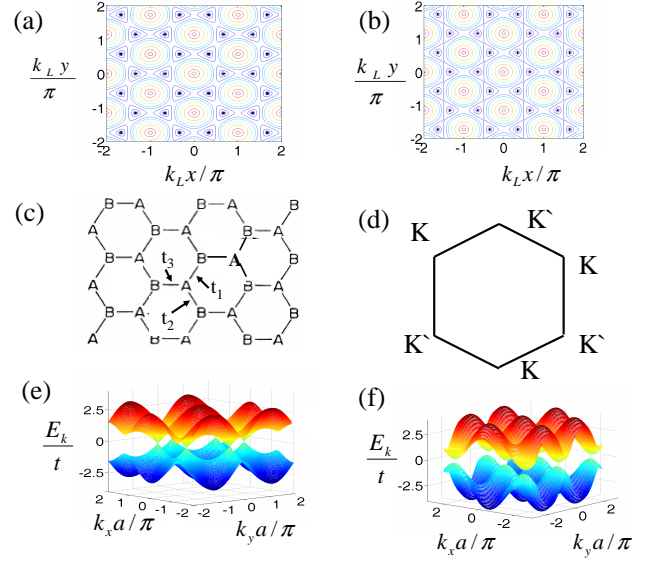


FIG. 1: (Color online) The hexagonal lattices. (a) and (b) The contours with three potentials described in Eq.(1). The minima of the potentials are denoted by the solid dots. All V_j^0 are the same in (a) and $V_1^0 = V_2^0 = 0.91V_3^0$ in (b). (c) Decomposition of the hexagonal lattice as two triangular sublattices A and B with anisotropic tunnelling. (d) The Brillouin zone of the hexagonal lattice. The dispersion relations are shown in (e) for $\beta = 1$ (gapless state) and (f) for $\beta = 2.5$ (gapped state).

q_x and q_y , the dispersion relation (3) becomes

$$E_{\mathbf{q}} = \pm \sqrt{\Delta^2 + v_x^2 q_x^2 + v_y^2 q_y^2}, \quad (4)$$

where $\Delta = 0$, $v_x = \sqrt{3}\beta ta/2$ and $v_y = ta\sqrt{1 - \beta^2/4}$ for $0 < \beta < 2$; and $\Delta = |t|(\beta - 2)$, $v_x = ta\sqrt{3\beta/2}$ and $v_y = ta\sqrt{\beta/2 - 1}$ for $\beta > 2$. This simplified dispersion relation $E_{\mathbf{q}}$ is actually a good approximation as long as $q_x, q_y \lesssim 1/2a$. We see that $E_{\mathbf{q}}$ represents the standard energy-momentum relation for the relativistic Dirac particles, with Δ taking the meaning of mass, and v_x and v_y replacing the light velocity. The wavefunction for the quasiparticles around the half filling then satisfies the Dirac equation $i\hbar\partial_t\Psi = H_D\Psi$, where the relativistic Hamiltonian H_D is given by

$$H_D = \alpha_0\Delta + v_x\alpha_x p_x + v_y\alpha_y p_y, \quad (5)$$

where the α_μ ($\mu = 0, x, y$) matrixes satisfy the Grassmannian algebra $\alpha_\mu\alpha_{\mu'} + \alpha_{\mu'}\alpha_\mu = 2\delta_{\mu\mu'}$, and for the 2+1 dimensional system, they can be taken as the three Pauli matrixes $\sigma_z, \sigma_x, \sigma_y$ [12].

In the above, through an analogy to the graphene physics, we have shown how to realize massive and massless Dirac fermions with cold atoms in an anisotropic hexagonal lattice. A more important question for this system, however, is how to experimentally verify the ex-

istence of these relativistic quasiparticles and the associated quantum phase transition. The detection method for ultracold atoms is very different from that for condensed matter materials, and the widely used technique based on the transport measurements for the latter is typically not available for the atoms. Nevertheless, there are some specific detection methods for the trapped atomic gas, and in the following we show how to confirm the relativistic quasiparticles and the phase transition with the density profile measurement [1, 16, 17] and the Bragg spectroscopy[15].

The density profile of the trapped atoms can be measured through the time-of-flight imaging with the light absorption. For free fermions, we have ballistic expansion, and from the final measured absorption images, one can reconstruct the initial real-space density profile of the trapped gas [17]. Now we show this density profile provides critical information for both massive and massless Dirac fermions. For trapped fermions, the local density approximation (LDA) is typically well satisfied, and under the LDA, the local chemical potential varies with the radial coordinate by $\mu = \mu_0 - V(\mathbf{r})$, where μ_0 is the chemical potential at the trap center and $V(\mathbf{r}) = m\omega^2\mathbf{r}^2/2$ is the global harmonic trapping potential [18]. So, μ is a monotonic function of r , and the density profile $n(r)$ is uniquely determined by the equation of the state $n(\mu)$.

For this system at temperature T , the atomic density (the number per unit cell) is given by

$$n(\mu) = \frac{1}{S_0} \int f(k_x, k_y, \mu) dk_x dk_y, \quad (6)$$

where $S_0 = 8\pi^2/\sqrt{3}a^2$ is the area of the first Brillouin zone of the honeycomb lattice, and $f(k_x, k_y, \mu) = 1/\{\exp[(E_{\mathbf{k}} - \mu)/T] + 1\}$ is the Fermi distribution. At low temperature ($T \sim 0$), this density profile $n(\mu)$ is shown in Fig. 2(a) and 2(b) for the parameters with massless and massive Dirac quasiparticles, respectively. One can clearly see that for the gapped phase with massive Dirac fermions, one has a plateau at the atom density $n = 1$ in the density profile. For the case with massless Dirac fermions, there is no such a plateau. So the plateau is associated with massive quasiparticles, and its emergence with tuning of the lattice anisotropy provides an unambiguous signal for the quantum phase transition between the two cases.

To further confirm the massless Dirac fermions, one needs to have evidence for their linear dispersion relation with the Dirac cone structure. At $T \sim 0$, $n(\mu)$ in Eq. (6) simplifies to $n(\mu) = (1/S_0) \int_{E_{\mathbf{q}} \leq \mu} dk_x dk_y$. Around the half filling ($n = 1$ which corresponds to the touching point in Fig. 1(e)), with a variation $\delta\mu$ in the chemical potential, $\delta n(\mu)$ geometrically represents the cross section of the Dirac cone, so it must be proportional to $(\delta\mu)^2$. In Fig. 2(c) and 2(d), we show the numerically calculated derivative of $n(\mu)$, and indeed at

the vicinity of the half filling, we see that $\frac{\partial n}{\partial \mu}$ is linearly proportional to $\delta\mu$ with the explicit asymptotic expression $\frac{\partial n}{\partial \mu} = \frac{4\pi}{v^2 S_0} |\delta\mu|$, where we have assumed the velocity $v_x = v_y = v$. So, experimentally, from the measured density profile $n(\mu)$, one can determine its slope. The latter quantity, with its linear form shown in Fig. 2(d), signals the linear dispersion relation around the Dirac cone, which confirms the massless Dirac fermions.

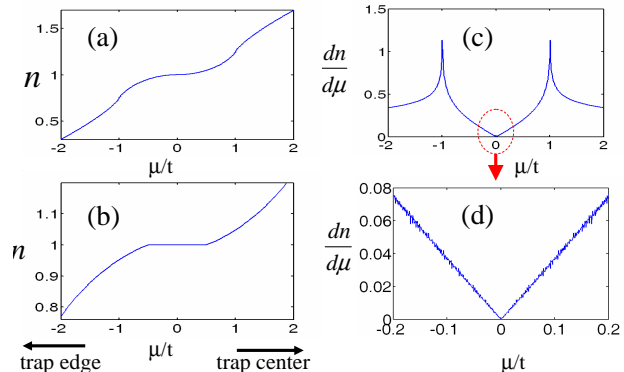


FIG. 2: (Color online) The number density of atoms n per unit cell as a function of the chemical potential μ (corresponding to a rescaled atomic density profile in a trap) for (a) $\beta = 1$, and (b) $\beta = 2.5$. A plateau with a width $2\beta - 4$ appears for the latter case which corresponds to the case when the chemical potential sweeps inside the energy gap. (c) The derivative $dn/d\mu$ as a function of the chemical potential μ for $\beta = 1$. (d) An enlarged part of $dn/d\mu$ at the vicinity of $\mu = 0$. The linearity of the curve shows the linear dispersion relation for the quasiparticles.

The Bragg spectroscopy can provide an alternative and complementary method to confirm the linear dispersion relation for the massless Dirac fermions and the energy gap for the massive ones. In Bragg spectroscopy[15], one shines two laser beams on the atomic gas as shown in Fig. 3a. By fixing the angle between the two beams (thus fixing the relative momentum transfer $\mathbf{q} = \mathbf{k}_2 - \mathbf{k}_1$, where \mathbf{k}_i denotes the wave vector of each laser beam), one can measure the atomic (or photonic) transition rate by scanning the laser frequency difference $\omega = \omega_2 - \omega_1$. From the fermi's golden rule, this transition rate basically measures the following dynamical structure factor [15]

$$S(\mathbf{q}, \omega) = \sum_{\mathbf{k}_1, \mathbf{k}_2} |\langle f_{\mathbf{k}_2} | H_B | i_{\mathbf{k}_1} \rangle|^2 \delta[\hbar\omega - E_{f_{\mathbf{k}_2}} + E_{i_{\mathbf{k}_1}}], \quad (7)$$

where $H_B = \sum_{\mathbf{k}_1, \mathbf{k}_2} \Omega e^{i\mathbf{q}\cdot\mathbf{r}} |i_{\mathbf{k}_1}\rangle \langle f_{\mathbf{k}_2}| + h.c.$ is the light-atom interaction Hamiltonian, and $|i_{\mathbf{k}_1}\rangle$ and $|f_{\mathbf{k}_2}\rangle$ denote the initial and the final atomic states with the energies $E_{i_{\mathbf{k}_1}}$ and $E_{f_{\mathbf{k}_2}}$ and the momenta \mathbf{k}_1 and \mathbf{k}_2 , respectively. At the half filling, the valence band (the lower half of Fig. 1(e) and 1(f)) is fully occupied, and the conduction band (the upper half) is empty. In that case, the excitations are dominantly around the touching point, and we can use the approximate dispersion relation in Eq.(4). For

the isotropic case ($\beta = 1$) with massless Dirac Fermions, we find $S(q, \omega)$ has the expression

$$S(q, \omega) = \begin{cases} 0, & (\omega \leq \omega_r) \\ \frac{\pi\Omega^2}{8v_F} \frac{2q_r^2 - q^2}{\sqrt{q_r^2 - q^2}}, & (\omega > \omega_r) \end{cases} \quad (8)$$

where $\omega_r = qv/\hbar$ ($q \equiv |\mathbf{q}|$) and $q_r = \hbar\omega/v$. This dynamical structure factor is shown in Fig. 3(b). Note that in this case, the lower cutoff frequency ω_r is linearly proportional to the momentum difference q , and ω_r vanishes when q tends to zero. The ratio between ω_r and q gives the fermi velocity v , an important parameter as the analogy of the light velocity for conventional relativistic particles. For the anisotropic case with $\beta > 2$, the spectrum in Eq. (4) becomes quadratic with $E \approx \pm(\Delta + \hbar^2 q_x^2/2m_x + \hbar^2 q_y^2/2m_y)$ for small momentum transfer \mathbf{q} , where the effective mass $m_{x,y} = \hbar^2\Delta/v_{x,y}^2$. The dynamic structure factor in this non-relativistic limit becomes

$$S(q, \omega) = \begin{cases} 0, & (\omega \leq \omega_c^{x,y}) \\ \frac{\pi\Omega^2\Delta}{2v_x v_y}, & (\omega > \omega_c^{x,y}) \end{cases} \quad (9)$$

where $\omega_c^{x,y} = 2\Delta + \hbar^2 q_{x,y}^2/4m_{x,y}$. Its form is shown in Fig. 3(b). The lower cutoff frequency $\omega_c^{x,y}$ in this case does not vanish as the momentum transfer go to zero. This distinctive difference between the dynamical structure factors in Eqs. (8) and (9) can be used to distinguish the cases with massive or massless Dirac fermions. From the variation of the cutoff frequency $\omega_c^{x,y}$ as a function of the momentum transfer $q_{x,y}$, one can also experimentally figure out the important parameters such as the energy gap Δ and the effective masses m_x and m_y .

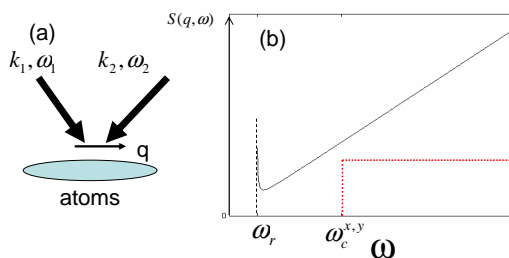


FIG. 3: (Color online) Schematic of the Bragg scattering. (a) Atoms are illuminated by two laser beams with wave vectors \mathbf{k}_1 , \mathbf{k}_2 and frequencies ω_1 , ω_2 , respectively. (b) The dynamic structure factors $S(q, \omega)$ (not scaled) for the massless Dirac fermions (solid line) and for the massive ones in the non-relativistic limit (dotted line). The experimentally measurable quantities ω_r and $\omega_c^{x,y}$ give important parameters for the quasiparticles.

In summary, we have proposed an experimental scheme to simulate and observe relativistic Dirac fermions and a

quantum phase transition with cold atoms in a (generally anisotropic) hexagonal optical lattice. The characteristic dispersion relations for the massless or the massive Dirac fermions can be confirmed through either the density profile measurement or the Bragg spectroscopy. The phase transition can be identified with the appearance of a plateau in the density profile as one tunes the lattice anisotropy. The appearance of relativistic quasiparticles, together with control of gauge fields for this system [19, 20], opens up the prospect to use the ultracold atoms to simulate some high energy physics.

This work was supported by the NSF under grant number 0431476, the ARDA under ARO contracts, the A. P. Sloan Foundation, the State Key Program for Basic Research of China (No. 2006CB921800), NCET and NSFC (Nos. 10674049, 10474034, and No. 60421003).

-
- [1] J.R. Anglin and W. Ketterle, *Nature* **416**, 211 (2002).
 - [2] I. Bloch, *Nature Phys.*, **1**, 23 (2005).
 - [3] D. Jaksch, et al., *Phys. Rev. Lett.* **81**, 3108 (1998).
 - [4] L.-M. Duan, E. Demler, and M. D. Lukin, *Phys. Rev. Lett.* **91**, 090402 (2003).
 - [5] E.Zhao and A.Paramakanti, *Phys. Rev. Lett.* **97**, 230404(2006); J. Ruostekoski, G.V. Dunne, and J. Javanainen, *ibid.* **88**, 180401 (2002).
 - [6] K. S. Novoselov *et al.*, *Nature* **438**, 197 (2005).
 - [7] Y. Zhang *et al.*, *Nature* **438**, 201 (2005).
 - [8] I. A. Lukyanchuk and Y. Kopelevich, *Phys. Rev. Lett.* **93**, 166402 (2004).
 - [9] M. I. Katsnelson, K. S. Novoselov, and A. K. Geim, *Nature Phys.* **2**, 620 (2006).
 - [10] C. L. Kane and E. J. Mele, *Phys. Rev. Lett.* **95**, 226801 (2005); L. Sheng *et al.*, *ibid.* **95**, 136602 (2005).
 - [11] V. P. Gusynin and S. G. Sharapov, *Phys. Rev. Lett.* **95**, 146801 (2005).
 - [12] G. W. Semenoff, *Phys. Rev. Lett.* **53**, 2449 (1984).
 - [13] I.M. Lifshitz, *Sov. Phys. JETP* **11**, 1130 (1960).
 - [14] X. G. Wen, *Quantum field theory of many-body systems* (Oxford University Press, Oxford, 2004).
 - [15] D. M. Stamper-Kurn *et al.*, *Phys. Rev. Lett.*, **83**, 2876 (1999).
 - [16] M. W. Zwierlein *et al.*, *Science* **311**, 492 (2006); G. B. Partridge *et al.*, *Science* **311**, 503 (2006).
 - [17] Y. Shin *et al.*, *Phys. Rev. Lett.* **97**, 030401 (2006).
 - [18] For simplicity, we assume here a specifically symmetric trap. Under the LDA, a non-spheric trap can be easily rescaled into a specific shape by redefine the unit of the length along different directions (see W. Yi and L. M. Duan, *Phys. Rev. A* **74**, 013610 (2006).).
 - [19] K. Osterloh *et al.*, *Phys. Rev. Lett.* **95**, 010403 (2005); J. Ruseckas *et al.*, *ibid.* **95**, 010404 (2005).
 - [20] D. Jaksch, P. Zoller, *New J. Phys.* **5**, 56 (2003); G. Juzeliunas and P. Ohberg, *Phys. Rev. Lett.* **93**, 033602 (2004); A. Sorensen, E. Demler, M. Lukin, *ibid.*, **94**, 086803 (2005); S. L. Zhu *et al.*, *ibid.*, **97**, 240401 (2006).